Journal of Materials Science: Materials in Electronics (2018) 29:13077–13086
https://doi.org/10.1007/s10854-018-9430-4

Transition metal (Mn) and rare earth (Nd) di-doped novel ZnO nanoparticles: a facile sol–gel synthesis and characterization

A. Albert manoharan[1] · R. Chandramohan[1] · K. Deva Arun Kumar[2] · S. Valanarasu[2] · V. Ganesh[3] · Mohd. Shkir[3] · H. Algarni[3] · S. AlFaify[3]

Received: 10 April 2018 / Accepted: 3 June 2018 / Published online: 9 June 2018

Abstract
Undoped, Mn doped and Nd co-doped ZnO nanoparticles are synthesized through a facile sol–gel route. Characterization of the synthesized samples has been done by X-ray diffraction, scanning electron microscopy, FT-IR, diffuse reflectance spectroscopy, photoluminescence spectroscopy, hall measurement and vibrating sample magnetometry. Structural and vibrational studies shown hexagonal wurtzite structure of prepared ZnO samples. SEM images have revealed that the grains are hexagonal and spherical shapes for undoped and co-doped samples. The crystallite size was found in range of 43–34 nm. The value of optical band gap is calculated and it is found ~ 3.27 eV for undoped and decreased to 3.20 eV for Mn doped, Nd co-doped sample. This tuning in band gap is because of the fact that the impurity band of ZnO is merged with the conduction band. Photoluminescence study reveals that the intensity of the prepared samples is systematically reduced with the addition of Mn and Nd doping element. Hall effect measurements reveal that the conductivity of ZnO nanoparticles is increased with respect to temperature. The magnetic measurements indicate that the obtained nanostructures are found to be room temperature ferromagnetism (RTFM) with maximum value of saturation magnetization for Nd co-doped Mn:ZnO nanoparticles, i.e. 2.44 emu g^{-1}. Thus the magnetic properties of ZnO prepared by low cost sol–gel method have been enhanced by Mn doping as well as Nd co-doping which can be used for spintronic applications. In future, similar rare earth materials could be considered for enhancing the magnetic properties of nano particles.

1 Introduction

Metal-oxide semiconductors (MOSs) play a vital role in various research fields particularly in spintronics, solar cells and gas sensors. These MOSs with the property of room temperature ferromagnetism (RTFM) are required for the working of the spintronic devices. A lot of research work is going on to achieve RTFM in MOS. These nano materials are synthesized in such a way that there are lot of intrinsic vacancies and are doped with diluted magnetic semiconductors (DMS) in little amount [1, 2]. These approaches will not only be helpful in spintronic devices but also in enhancing gas sensing properties of the material [3, 4]. Zinc oxide (ZnO) is II–VI compound semiconductor and low threshold power for optical pumping [5–8]. This is suitable for a widespread series of technological requests particularly in short wavelength light emitting devices due to its optical transparency, wide energy gap (3.37 eV), and larger exciting binding energy (60 meV) [9]. Moreover, many intrinsic properties of ZnO such as broad range of radiation absorption, large electrochemical coupling coefficients and high photostability makes it a best candidate for short wavelength optoelectronic and photonic devices [10–14]. Zinc oxide properties could be modified with the change in its crystal size, structure, aspect ratio, density, orientation and morphology. Recently, many researchers have studied ZnO nanoparticles for electrochemical behavior [15], magnetic behavior like: ferromagnetism [16] and spin glass behavior [17]. Nirmala et al. [18] reported the ZnO nanoparticles prepared by DC thermal

✉ R. Chandramohan
rathinam.chandramohan@gmail.com

✉ Mohd. Shkir
shkirphysics@gmail.com

[1] PG and Research Department of Physics, Sree Sevugan Annamalai College, Devakottai 630303, India

[2] PG and Research Department of Physics, Arul Anandar College, Karumathur, Madurai 625514, India

[3] Advanced Functional Materials and Optoelectronics Laboratory (AFMOL), Department of Physics, College of Science, King Khalid University, P.O. Box 9004, Abha 61413, Saudi Arabia

plasma method have modified their properties on doping with Mn and Co. Recently, many scientists have synthesized the rare earth elements such as Gadolinium (Gd), Lanthanum (La), and Neodymium (Nd) doped with the wide band gap semiconductors (ZnO, SnO_2) materials for improving the magnetization properties [19, 20]. Among these rare earth elements, Nd is one of best due to its unique optical and magnetic characteristics. The ionic radius of Nd^{3+} (0.98 Å) is higher than the ionic radius of Zn^{2+} (0.74 Å), hence the Zn ions can be easily replaced by Nd ions with some minor change in the crystal structure.

A wide range of synthetic methods has been used to prepare the nanoparticles such as aspalathus linearis natural extracts [21], co-precipitation method [22], moringa oleifera green synthesis [15], and sol–gel method [23, 24]. Among these methods, sol–gel method attracts more attention due to its unique advantages including simple lab equipment, low cost, easy to handle and ability to produce large amount of nanoparticles (NPs) etc.

In this research work, simple sol–gel technique is used to prepare the undoped, Mn doped and Nd co-doped ZnO nanoparticles. As per existing literature this is going to be first novelty report on synthesis of Nd co-doped Mn:ZnO nanoparticles using a simple sol–gel route for spintronics applications. After the completion of the preparation process, the sample was stored in room temperature for further characterization. Characterization has been done to investigate its structural, optical, electrical and magnetic properties.

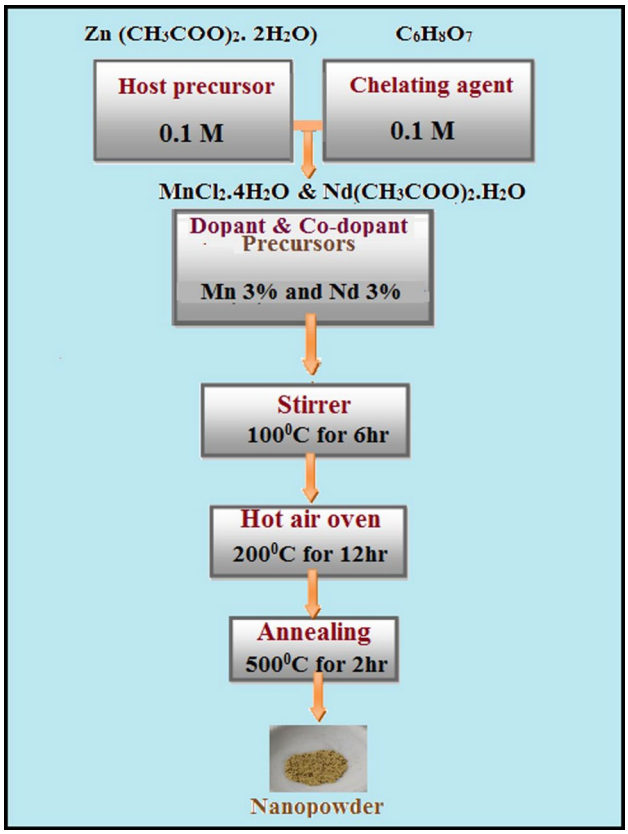

Fig. 1 The layout diagram of doped ZnO nanopowder preparation process

2 Experimental procedure

In a typical synthesis procedure, Zinc acetate dihydrate [Zn $(CH_3COO)_2{\cdot}2H_2O$], Manganese(II) chloride tetrahydrate [$MnCl_2{\cdot}4H_2O$], Neodymium acetate hydrate [$Nd(CH_3COO)_2{\cdot}H_2O$] and citric acid ($C_6H_8O_7$) were used as starting materials. Required amounts (0.1 M) of materials were liquefied in distilled water. Host precursor solution and citric acid were then added in 1:1 molar ratio. The amount of Mn and Nd dopant concentration added was 3%. The magnetic stirrer was used to stir the solution at 100 °C for 6 h and stirring continued till the formation of gel. After the formation of gel, it was allowed to burn at 200 °C for 12 h using hot air oven. As a result of combustion, light fluffy mass was obtained. Further annealing is done at 500 °C for 2 h to acquire crystalline ZnO nanoparticles. Layout diagram for the preparation of Nd co-doped Mn:ZnO nanopowder is depicted in Fig. 1. The prepared doped ZnO samples were subjected to X-ray diffraction (XRD), scanning electron microscopy (SEM), Fourier transform infra red spectroscopy (FTIR), diffuse reflectance spectroscopy (DRS), photo luminescence spectroscopy (PL), hall measurement employing two probe methods and vibrating sample magnetometry (VSM) measurements. XRD method using Cu-Kα radiations (λ = 0.15406 nm) in 20°–80° region is used to analyze the crystallinity and crystallite size of the prepared nano particles. The SEM studies help in analyzing the morphology of the sample with EDAX in compositional analysis. FTIR Spectrum 65, Perkin Elmer in the region of 100–4000 cm^{-1} with a resolution of 1 cm^{-1} is used to obtain FTIR spectra of the prepared samples. PL spectrometer (LS-55B, Perkin Elmer) with a Xenon lamp as source is applied. For this experiment, the excitation wavelength used was 325 nm. Electrical and magnetic studies were also carried out using Keithley source meter (2450) and vibrating sample magnetometer (VSM, Lakeshore-7400, USA) respectively.

3 Results and discussion

3.1 Structural studies

Figure 2 depicts XRD patterns of ZnO samples with 3% Mn and Nd doping concentrations which were prepared by sol–gel method with a fixed annealing temperature at 500 °C for 2 h. The observed characteristic peaks with high

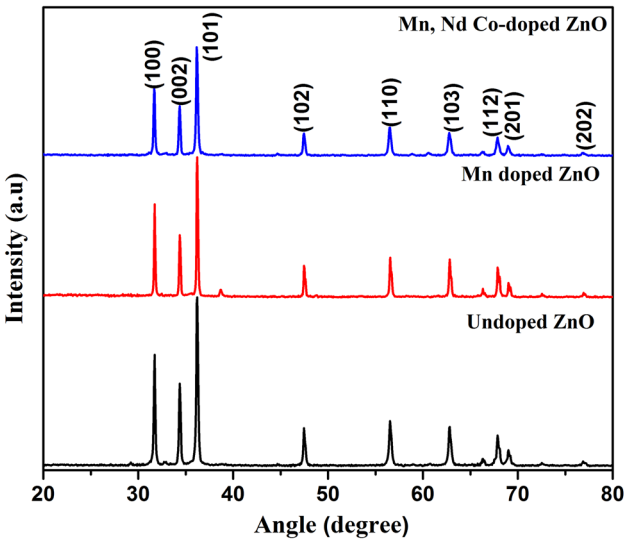

Fig. 2 XRD pattern of undoped, doped and co-doped ZnO nanoparticles

intensities at (100), (002), (101) planes and low intensities at (102), (110), (103), (112), (201), (004) (202) planes of ZnO were matched well with JCPDS card no: 89-1397 which indicates that the samples are of high-purity and the structure of ZnO is hexagonal wurtzite. The XRD spectrum shows a prominent peak in the (101) plane for all the undoped and doped ZnO samples. It indicates that the plane has minimum surface energy [25] to orient the crystallites strongly in the plane (101) compared to others. From the XRD data, it has been observed that there is no detected extra peak corresponding to the secondary-phase formation for 3% of Mn doped sample. This means that the wurtzite structure does not change by the doped Mn ions. Poornaprakash et al. [26] also reported same result for Mn doped ZnO nanoparticles via hydrothermal method. Further, the XRD pattern of Nd co-doped with Mn:ZnO nanoparticles indicates that there is no Nd related impurity peak. Because, the Nd ions are intestinally incorporated within the Mn and Zn sites due to the higher ionic radius of Nd. However, from the XRD spectrum it is clearly observed that the crystalline nature of the ZnO sample is slightly affected by the inclusion of Mn, Nd elements. Such decrease in crystalline nature with Mn and Nd incorporation has been reported earlier [27, 28].

XRD peak profiling for the high-intensity peak (101) was used to determine the size of crystallite for the prepared doped ZnO nano particles. The size of the crystallite D was calculated by the relation [29–31]:

$$D = \frac{k\lambda}{\beta \cos\theta} \tag{1}$$

Here all symbols are of usual meanings. The decreasing diffraction peak (101) intensity indicates nano crystallinity

Table 1 Structural parameters of undoped and doped ZnO nanoparticles

ZnO nanoparticles	Crystallite size (nm)	Lattice parameter JCPDS (no.: 89-1397)		v (Å^3)
		a (Å)	c (Å)	
Undoped	42.5	3.254	5.19	47.85
Mn doped	37.6	3.253	5.217	47.83
Mn, Nd co-doped	34.0	3.252	5.211	47.73

of samples. Also it is found that size of crystallites is lessened with addition of Mn doping element due to the increase in β with respect to Mn doping. In addition, the inclusion of Nd co-dopant ions reduces the size of crystallites again due to the increase of disorder effect.

The lattice constants "*a*" and "*c*" and unit cell volume "*V*" of the hexagonal phase structure of doped ZnO nano particles were determined by the relation [32] using XRD data.

$$\frac{1}{d^2} = \frac{4}{3}\left\{\frac{h^2 + hk + k^2}{a^2}\right\} + \left\{\frac{l^2}{c^2}\right\} \tag{2}$$

The lattice constants were calculated by taking an average of all the observed X-ray diffraction peaks and are shown in Table 1. It can be extracted from tabulated data that lattice constants of Nd co-doped Mn:ZnO nanoparticles are slightly larger than the standard JCPDS parameters for bulk ZnO. This might be due to fact that ionic radii of Nd^{3+} (0.98 Å) and Mn^{2+} (0.72 Å) are larger than that of Zn^{2+} (0.74 Å) [33]. It is also found that the value of "*a*" and "*v*" are increased with addition of Mn and Nd co-doping concentrations.

Generally, if we change the temperature for solution phase synthesis the crystalline nature can be significantly change. In our case, the solution temperature is constant for synthesis process so there is no significant effect in the crystalline nature in XRD study. At the same time, the ZnO crystallinity was slightly reduced is may be due to the addition of various doping (Mn) and co-doping (Nd) elements into the host zinc (Zn) material.

3.2 SEM with EDAX analysis

Figure 3a–c depicts SEM of undoped, Mn doped and Nd co-doped ZnO nanoparticles. We observed that for undoped ZnO as shown in Fig. 3a, the particle size is higher than that of doped ZnO sample. The undoped ZnO image shows that the powder is grown in huge size in the form of hexagonal shaped particles and is uniformly presented as supported by our XRD. The uniform distribution of hexagonal shaped particles is slightly reduced on adding 3% Mn as shown in

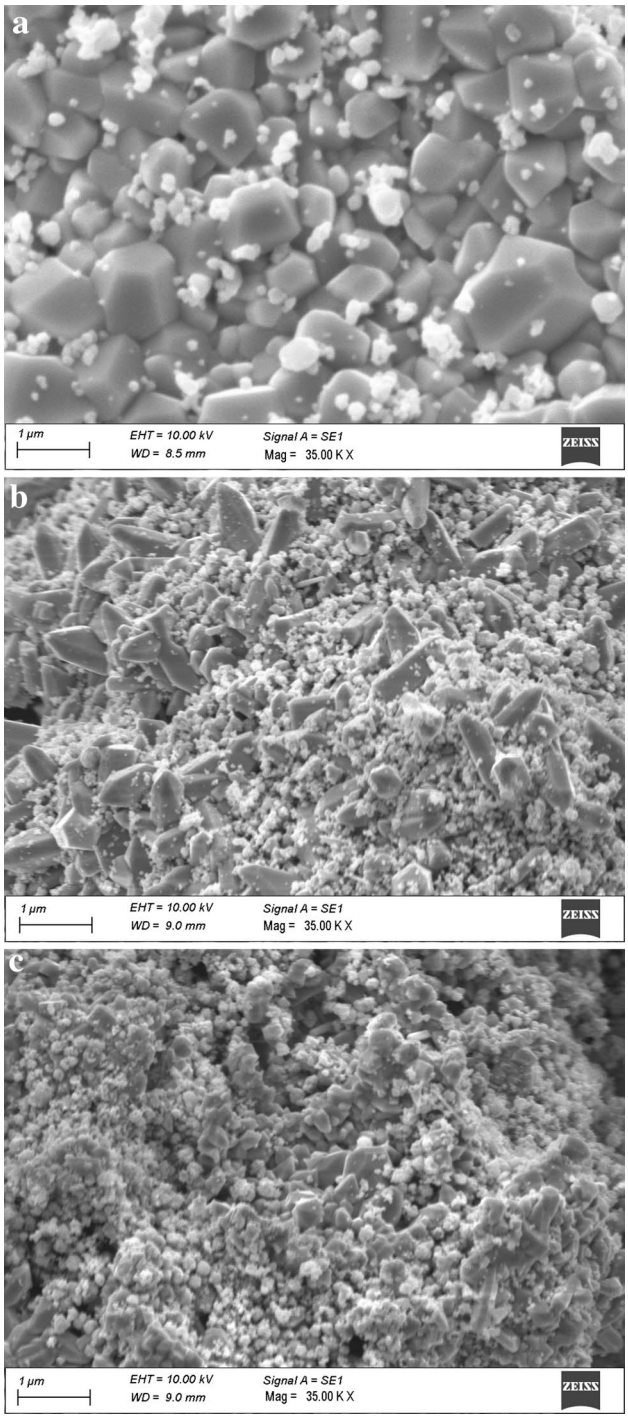

Fig. 3 SEM images of **a** undoped, **b** Mn doped, **c** Mn, Nd co-doped ZnO nanoparticles

Fig. 3b, which is due to the change in strain level on Mn doping. In addition, the shape and size of the particles are totally changed from hexagonal to spherical with the addition of rare earth neodynum (Nd) co-doping element. Due to the Nd ions incorporation, particle size and ionic radius of metallic ions are inversely relative [34]. Further, the image shows that the particles are spherical shaped grains and well-defined grain boundaries. The reduction of particle sizes are 95, 70 and 55 nm for undoped, Mn doped and Nd co-doped ZnO samples respectively due to decrease in number of surface atoms for doping impurities in ZnO nanoparticles. However, few pinholes are found in the Nd co-doped Mn:ZnO nanoparticles which may be due to the surface deficiency. The observed SEM results match with the previous report by Sharma et al. [35].

Figure 4a depicts the elemental (SEM overview) mapping images of Nd co-doped Mn:ZnO nanoparticles. Zinc, Oxygen, Manganese and Neodymium elements are uniformly distributed over the surface of Nd:Mn:ZnO nanopowder. Figure 4b shows the elemental compositional analysis of EDAX spectrum for Nd co-doped Mn:ZnO nanoparticles. The EDAX spectrum shows the occurrence of Zn, O, Mn and Nd in prepared sample. The quantifiable EDAX displays that Zn, O, Mn and Nd are 42.8, 52.5, 2.2 and 2.5% respectively.

3.3 FTIR spectroscopy

The chemical, structural nature of prepared ZnO nanoparticles can be studied by FTIR analyses. Figure 5 represents the FTIR spectrum recorded for the ZnO nanoparticles from 100 to 4000 cm^{-1}. FTIR spectrum displays a strong peak at 470 cm^{-1} corresponding to formation of Zn–O bond [36]. The FTIR spectra of undoped, Mn doped and Nd co-doped Mn:ZnO nanoparticles show two strong absorption bands at 435[1], 434, 426 and 505, 487, 486 cm^{-1}, respectively. The strong absorption bands at 505, 487, 486 cm^{-1} are observed due to lack of oxygen and its vacancy (VO) defect complex in ZnO while bands at 435, 434, 426 cm^{-1} may be owed to E_2 mode of hexagonal ZnO [37]. Peak at 2331 cm^{-1} is assigned to C=O stretching vibrations. Broad peak at 3475 cm^{-1} is allocated to O–H stretching of hydroxyl group absorbed on surface. O–H peak at 3456 cm^{-1} is associated with defects and density of free carriers [38]. Results of FTIR confirmed the results of XRD analysis. The facts obtained from the FTIR regarding the surface area and surface defects make us to recognize the sensing conduct of prepared ZnO nanoparticles.

3.4 Optical studies

Diffuse reflectance spectroscopy (DRS) spectra of all samples are depicted in Fig. 6 within the wavelength range of 350–850 nm. The observed reflectance was systematically decreased with the addition of Mn doped and Nd co-doped ZnO nanoparticles. From the reflectance spectra, the absorption edge of the Mn doped and Nd co-doped samples shifted slightly to higher wavelengths compared to undoped ZnO. The absorption edges are observed at 356, 362 and 364 nm for

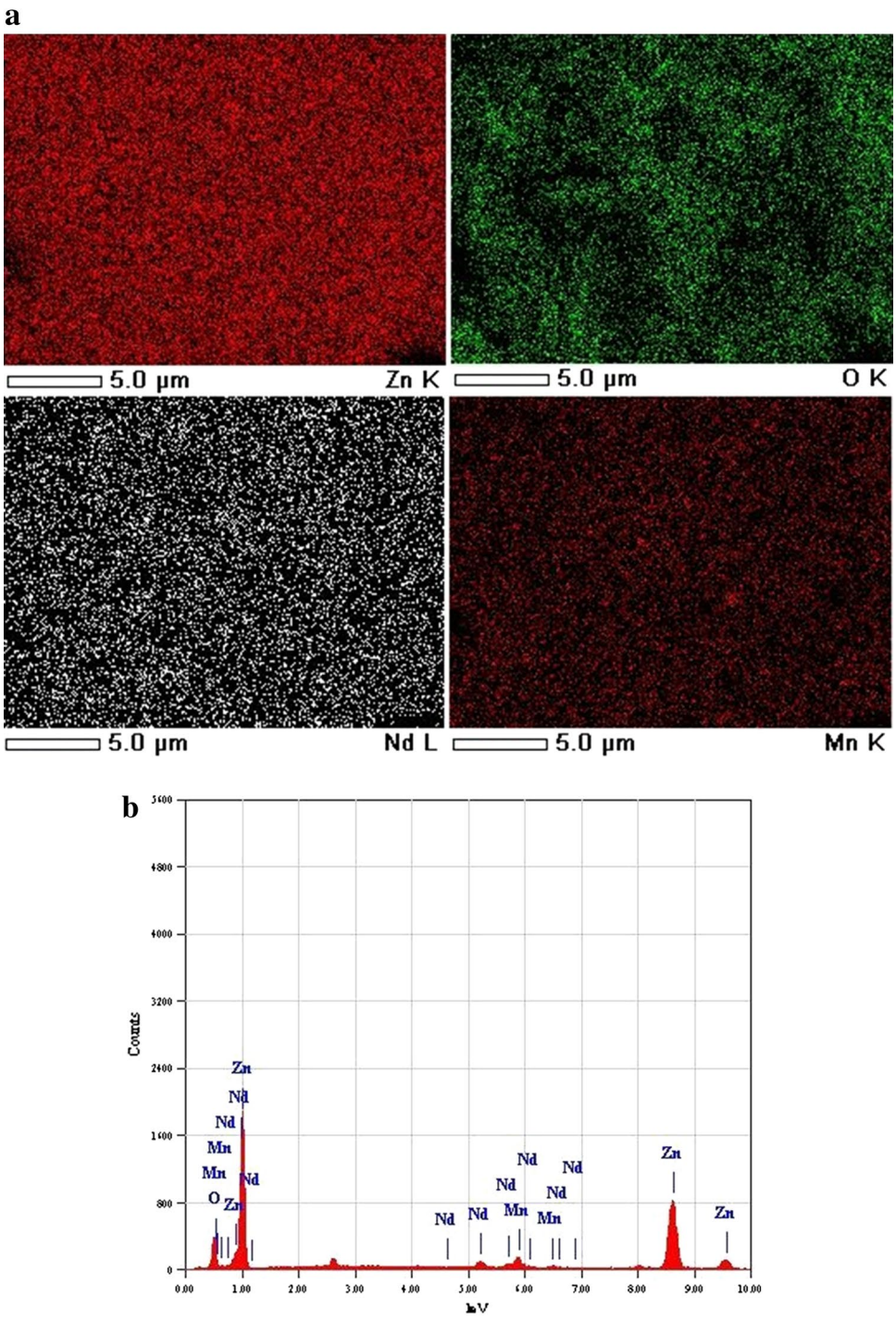

Fig. 4 **a** SEM mapping image and **b** EDAX spectrum of Mn, Nd co-doped ZnO nanoparticles

undoped, Mn doped and Nd co-doped ZnO correspondingly. Observed absorption edge in spectra of Mn:ZnO nanopowder possibly linked to intra-band gap transitions together with oxygen vacancies and Zn interstitials with diverse charge states.

The optical band gap has been calculated according to the expression by Tauc relation for all samples [26, 39–41]:

$$\left[F(R)h\nu/t\right]^{1/n} = A(h\nu - E_g) \quad (3)$$

where A is proportional constant, E_g is band gap, hν is photon energy, n = 1/2 for the direct band gap and F(R) is the Kubelka–Munk function. Kubelka–Munk function can be defined as the relation of $F(R) = (1-R)^2/2R$, where R is diffused reflectance in UV–Vis spectra. The estimated values of the energy band gap (Eg) of prepared ZnO samples were shown in Fig. 7. The direct energy gap is decreased from 3.27 to 3.20 eV for the undoped to co-doped ZnO samples respectively. Direct band gap value was decreased because

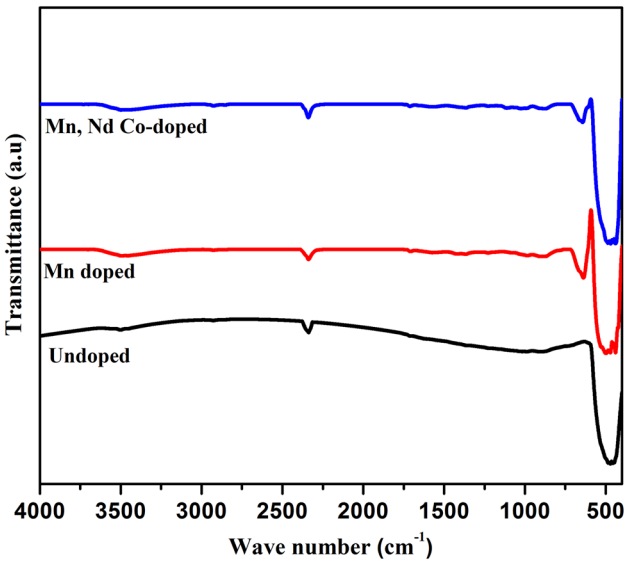

Fig. 5 FTIR spectrum of undoped and doped ZnO nanoparticles

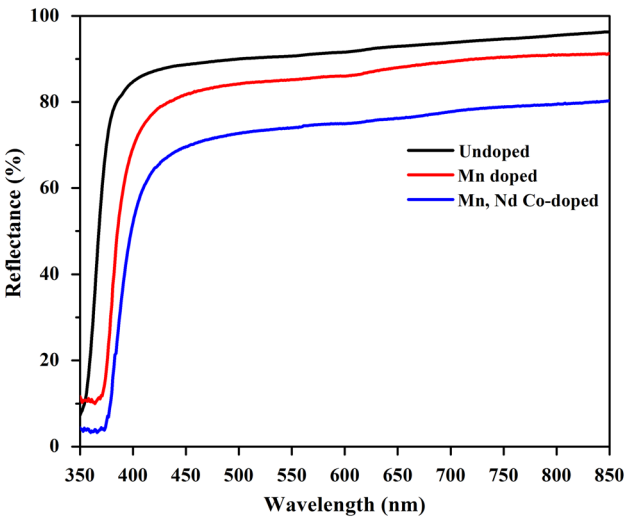

Fig. 6 Reflection spectra of undoped and doped ZnO nanoparticles

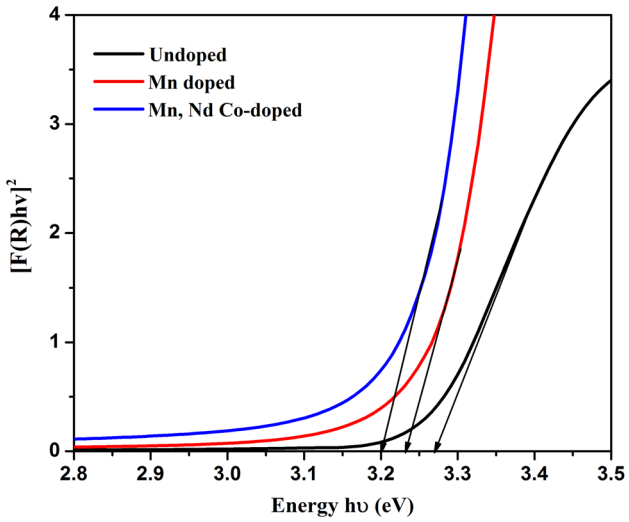

Fig. 7 Band gap variations of undoped and doped ZnO nanoparticles

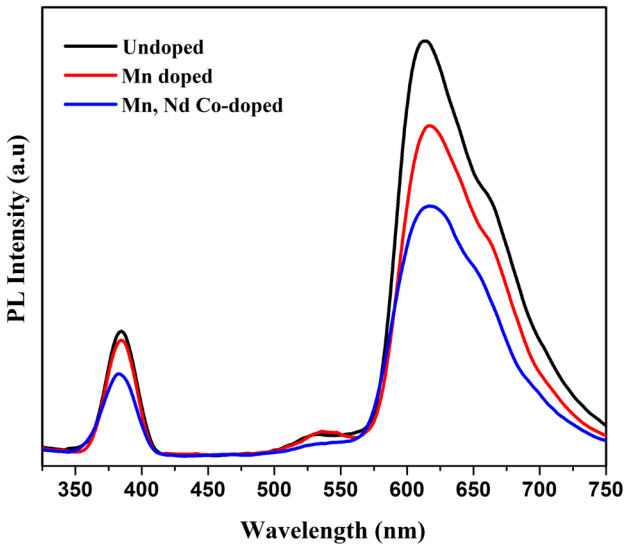

Fig. 8 PL spectra of undoped and doped ZnO nanoparticles

the electronic structure of the samples was changed due to the strain on doping [42]. Here the decrease in band gap i.e. band gap narrowing effect (BGN) is due to tensile lattice strain. Such energy gap narrowing may be enlightened as electron–electron and electron–impurity scattering when levels of doping are well beneath Mott's critical density.

3.5 Photoluminescence analysis

PL is used to study optical properties of materials at molecular levels. PL is also used to determine the band gap energy, probe evolution of electron–hole surface of semiconductors and identify precise defects of radioactive transitions and impurity levels [43, 44]. It is learned from previous reports that the emission wavelength of semiconductor oxide is affected by several factors including the concentration of the dopant, particle's morphology, size, and wavelength of excitation [45]. Figure 8 depicts luminescence spectra of prepared ZnO nanoparticles. There are two emission regions: ultraviolet and visible regions in ZnO nanoparticles [46]. In the visible region, there is a decrease in the PL intensity with the addition of doped and co-doped elements. This is because of the substitution of Mn^{2+} and Nd^{3+} ions for Zn^{2+} ions, (good agreement with Fig. 2). Moreover, the red shift phenomena take place due to the strong visible emission peak at 615 nm. In ultraviolet region, expansion of emission band is more for doped ZnO samples than that of pure ZnO.

This expansion may be due to the presence of –OH group and the introduction of defects by doping of Mn and Nd. As a result, there is an increase in the recombination processes of holes in valence band as well as in band-edge excitation of ZnO with electrons in conduction band. The observed UV emission peak at 384 nm is well agreed with the previous report on ZnO [47, 48].

3.6 Electrical analysis

The temperature dependence of electrical conductance for prepared samples of ZnO nano particles is depicted in Fig. 9. It is seen that the conductivity is high for undoped ZnO nanoparticles and low for doped ZnO samples. The electrical conductivity takes place in undoped ZnO at 300 K as intrinsic defects formed through oxygen vacancies and such defects cause donor states in forbidden band somewhat beneath of conduction band which lead to the conducting behavior of ZnO. These intrinsic defects in undoped ZnO samples are generated during synthesis. While preparing the sample, usually a high temperature (more than 1000 °C) will be produced during combusting process. This high temperature produces oxygen vacancies in the sample which cause electrical conductivity. The lessening of in ZnO conductivity on Mn doping leads to conclusion that Mn doping disturbs the intrinsic defects in the ZnO [49]. The Mn in ZnO acts as a deep donor which cause in lessening the density of intrinsic donors at incineration temperature ensuing in decrease of electrical conductivity. Also, the intrinsic donor concentration in the sample is further decreased on the addition of Nd co-doping level, which leads to further decrease in electrical conductivity of prepared sample. Besides the decrease in conductivity, the samples shows semiconducting behavior with increase of temperature. Moreover, based on conductivity variation, conductivity curve can be divided into two regions. One of them may be ascribed to extrinsic conductivity region (lower temperature) and the other to intrinsic conductivity region (higher temperature). It is seen for pure ZnO, the increase in conductivity is observed slowly with increase of temperature up to 420 K, and later the conductivity is increased drastically. The conductivity of Mn doped and Nd co-doped ZnO sample was also varied slowly up to 420 K, later it increases drastically.

3.7 Magnetic properties

Figure 10 shows the M(H) curves of Mn doped, Nd co-doped ZnO nanoparticles. The decent hysteresis behavior is realized at 300K in this curve. It is known that pure ZnO behaves like anti-ferromagnetic material [50, 51], and magnetic properties are determined by their size [52]. Inset of Fig. 10 depicts magnetic curve of pure ZnO nanoparticles. As predictable, value of magnetic moment is 1.05 (emu g^{-1}) which is better than the previous reports. The ferromagnetic ordering starts to occur at room temperature on the inclusion of doping element because of doping mechanism of Mn^{2+} ions into the nanostructure of doped ZnO. It implies that the magnetic properties of doped ZnO are high compared to pure ZnO. Doped and co-doped elements causes increase in magnetic moment as seen from the Table 2. Rao et al. [53] reported that the ferromagnetic properties in Mn-doped ZnO nanostructures are due to double exchange mechanism by the coexistence of Mn^{2+} and Mn^{3+} ions. Moreover it is found that there is an exchange and the interaction of Zn–O–Zn bond. According to Zhao et al. [54], the source of ferromagnetic chattels in Mn-doped ZnO lies in super-exchange collaboration of Mn–O–Zn–O–Mn coupling. Also, somewhat

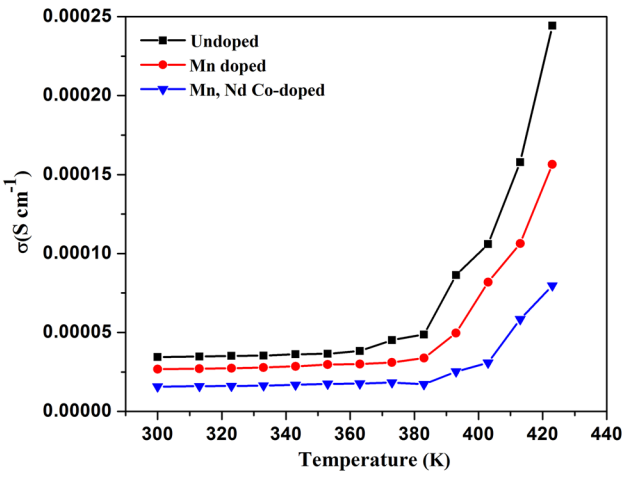

Fig. 9 Electrical conductivity variation versus temperature of doped ZnO nanoparticles

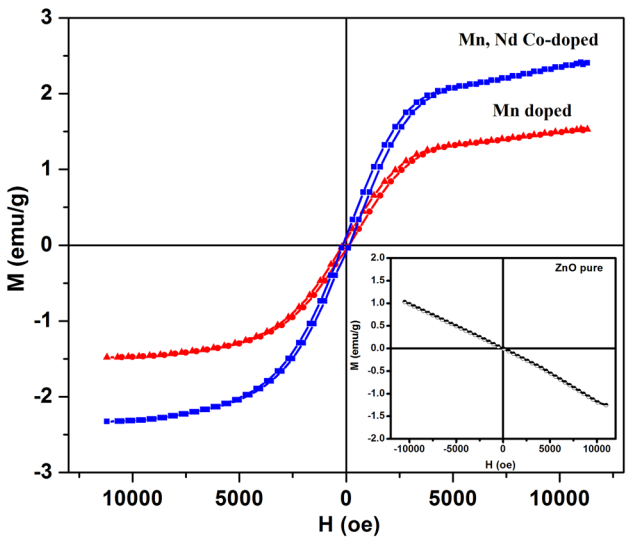

Fig. 10 Magnetization curves of pure and doped ZnO nanoparticles

Table 2 Magnetic properties of doped and co-doped ZnO nanoparticles

ZnO nanoparticles	H_c (Oe)	M_r (emu g^{-1})
Mn doped	11,335	1.56
Mn, Nd co-doped	11,340	2.44

improved hysteresis performance of Nd co-doped sample is observed because Nd–O–Mn–O–Nd couplings increase with the Nd co-doped sample. Furthermore, the amount of oxygen vacancies is frolicked a key character in interceding ferromagnetism conversation between Nd^{3+} and Mn^{2+}. More oxygen vacancies might have been generated on doping with Nd ions which are responsible for pragmatic wide assortment ferromagnetic order. In our case, observed long range ferromagnetic behavior in Nd co-doped Mn:ZnO sample might be due to defects like oxygen vacancies and it is reliable with bound magnetic polarons (BMP) model [55]. Similar result was also reported by Kumar et al. [56] for Nd doped ZnO. It is also found that the ferromagnetism in the prepared samples is vanished at low temperature. It is observed at 77 K, the hopping behavior ceases, and thus no ferromagnetism is observed. Such behavior already observed by Bhowmik et al. for α-Fe_2O_3 [57], at low temperature does not show any ferromagnetic behavior, which is confirming the antiferromagnetic order. Hence room temperature ferromagnetism is developed in the sample, which could be considered as a potential candidate for spin based applications.

4 Conclusions

Undoped, doped and co-doped ZnO nanopowders were successfully prepared using sol–gel method. Single phase ZnO nanoparticles is found by XRD. No impurity phase was observed in XRD for both doped and co-doped samples. The lattice parameters were slightly decreased for Nd co-doped Mn:ZnO sample. FTIR studies confirmed the fact that the defects are more in undoped ZnO than the doped ZnO as indicated by XRD results. The PL studies supported the XRD results that the particle size is decreased with respect to different doping elements. The optical studies showed that the band gap of the doped samples is reduced. Electrical studies revealed that conductivity increases with increasing temperature. Magnetic studies reported that the magnetic moment was higher for Nd co-doped Mn:ZnO nanoparticles. In conclusion, the Mn and Nd doped ZnO nanomaterial can improve the optical, electrical and magnetic properties by sol–gel route.

Acknowledgements The authors would like to express their gratitude to Deanship of Scientific Research at King Khalid University for funding this work through Research Groups Program under Grant No. R.G.P. 1/54/39.

Compliance with ethical standards

Conflict of interest Authors declares that there is no conflict of interest involve in the current work.

References

1. G. Xing, D. Wang, J. Yi, L. Yang, M. Gao, M. He, J. Yang, J. Ding, T.C. Sum, T. Wu, Correlated d_0 ferromagnetism and photoluminescence in undoped ZnO nanowires. Appl. Phys. Lett. **96**, 112511 (2010)
2. U. Philipose, S.V. Nair, S. Trudel, C. De Souza, S. Aouba, R.H. Hill, H.E. Ruda, High-temperature ferromagnetism in Mn-doped ZnO nanowires. Appl. Phys. Lett. **88**, 263101 (2006)
3. Y. Zhang, J. Xu, Q. Xiang, H. Li, Q. Pan, P. Xu, Brush-like hierarchical ZnO nanostructures: synthesis, photoluminescence and gas sensor properties. J. Phys. Chem. C **113**, 3430–3435 (2009)
4. L. Liu, S. Li, J. Zhuang, L. Wang, J. Zhang, H. Li, Z. Liu, Y. Han, X. Jiang, P. Zhang, Improved selective acetone sensing properties of Co-doped ZnO nanofibers by electrospinning. Sens. Actuators B **155**, 782–788 (2011)
5. P. Zu, Z. Tang, G.K. Wong, M. Kawasaki, A. Ohtomo, H. Koinuma, Y. Segawa, Ultraviolet spontaneous and stimulated emissions from ZnO microcrystallite thin films at room temperature. Solid State Commun. **103**, 459–463 (1997)
6. D. Bagnall, Y. Chen, Z. Zhu, T. Yao, S. Koyama, M.Y. Shen, T. Goto, Optically pumped lasing of ZnO at room temperature. Appl. Phys. Lett. **70**, 2230–2232 (1997)
7. M. Kawasaki, A. Ohtomo, I. Ohkubo, H. Koinuma, Z. Tang, P. Yu, G. Wong, B. Zhang, Y. Segawa, Excitonic ultraviolet laser emission at room temperature from naturally made cavity in ZnO nanocrytal thin films. Mater. Sci. Eng. B **56**, 239–245 (1998)
8. A. Ohtomo, M. Kawasaki, I. Ohkubo, H. Koinuma, T. Yasuda, Y. Segawa, Structure and optical properties of ZnO/$Mg_{0.2}Zn_{0.8}O$ superlattices. Appl. Phys. Lett. **75**, 980–982 (1999)
9. K.D.A. Kumar, V. Ganesh, M. Shkir, S. AlFaify, S. Valanarasu, Effect of different solvents on the key structural, optical and electronic properties of sol–gel dip coated AZO nanostructured thin films for optoelectronic applications. J. Mater. Sci. Mater. Electron. **29**, 887–897 (2018)
10. Ü Özgür, Y.I. Alivov, C. Liu, A. Teke, M. Reshchikov, S. Doğan, V. Avrutin, S.-J. Cho, H. Morkoc, A comprehensive review of ZnO materials and devices. J. Appl. Phys. **98**, 041301 (2005)
11. K.D.A. Kumar, S. Valanarasu, A. Kathalingam, V. Ganesh, M. Shkir, S. AlFaify, Effect of solvents on sol–gel spin-coated nanostructured Al-doped ZnO thin films: a film for key optoelectronic applications. Appl. Phys. A **123**, 801 (2017)
12. K.D.A. Kumar, S. Valanarasu, V. Ganesh, M. Shkir, A. Kathalingam, S. AlFaify, Effect of precursors on key opto-electrical properties of successive ion layer adsorption and reaction-prepared Al:ZnO thin films. J. Electron. Mater. **47**, 1335–1343 (2018)
13. Y.W. Heo, D. Norton, L. Tien, Y. Kwon, B. Kang, F. Ren, S. Pearton, J. LaRoche, ZnO nanowire growth and devices. Mater. Sci. Eng. R **47**, 1–47 (2004)
14. G.-C. Yi, C. Wang, W.I. Park, ZnO nanorods: synthesis, characterization and applications. Semicond. Sci. Technol. **20**, S22 (2005)
15. N. Matinise, X. Fuku, K. Kaviyarasu, N. Mayedwa, M. Maaza, ZnO nanoparticles via *Moringa oleifera* green synthesis: physical

properties & mechanism of formation. Appl. Surf. Sci. **406** 339–347 (2017)
16. S. Jung, S.-J. An, G.-C. Yi, C. Jung, S.-I. Lee, S. Cho, Ferromagnetic properties of $Zn_{1-x}Mn_xO$ epitaxial thin films. Appl. Phys. Lett. **80**, 4561–4563 (2002)
17. Z. Jin, T. Fukumura, M. Kawasaki, K. Ando, H. Saito, T. Sekiguchi, Y. Yoo, M. Murakami, Y. Matsumoto, T. Hasegawa, High throughput fabrication of transition-metal-doped epitaxial ZnO thin films: a series of oxide-diluted magnetic semiconductors and their properties. Appl. Phys. Lett. **78**, 3824–3826 (2001)
18. M. Nirmala, P. Smitha, A. Anukaliani, Optical and electrical properties of undoped and (Mn, Co) co-doped ZnO nanoparticles synthesized by DC thermal plasma method. Superlattices Microstruct. **50**, 563–571 (2011)
19. M. Ungureanu, H. Schmidt, Q. Xu, H. von Wenckstern, D. Spemann, H. Hochmuth, M. Lorenz, M. Grundmann, Electrical and magnetic properties of RE-doped ZnO thin films (RE = Gd, Nd). Superlattices Microstruct. **42**, 231–235 (2007)
20. Q. Xu, H. Schmidt, H. Hochmuth, M. Lorenz, A. Setzer, P. Esquinazi, C. Meinecke, M. Grundmann, Room temperature ferromagnetism in Nd-and Mn-codoped ZnO films. J. Phys. D. **41**, 105012 (2008)
21. A. Diallo, B. Ngom, E. Park, M. Maaza, Green synthesis of ZnO nanoparticles by *Aspalathus linearis*: structural & optical properties. J. Alloy. Compd. **646**, 425–430 (2015)
22. M. Arularasu, M. Anbarasu, S. Poovaragan, R. Sundaram, K. Kanimozhi, C.M. Magdalane, K. Kaviyarasu, F. Thema, D. Letsholathebe, G.T. Mola, Structural, optical, morphological and microbial studies on SnO_2 nanoparticles prepared by co-precipitation method. J. Nanosci. Nanotechnol. **18**, 3511–3517 (2018)
23. K. Kaviyarasu, P. Murmu, J. Kennedy, F. Thema, D. Letsholathebe, L. Kotsedi, M. Maaza, Structural, optical and magnetic investigation of Gd implanted CeO_2 nanocrystals. Nuclear Instrum. Methods Phys. Res. Sect. B **409**, 147–152 (2017)
24. K. Kaviyarasu, P.A. Devarajan, A convenient route to synthesize hexagonal pillar shaped ZnO nanoneedles via CTAB surfactant. Adv. Mater. Lett. **4**, 582–585 (2013)
25. Y. Morinaga, K. Sakuragi, N. Fujimura, T. Ito, Effect of Ce doping on the growth of ZnO thin films. J. Crystal Growth **174**, 691–695 (1997)
26. B. Poornaprakash, U. Chalapathi, S. Babu, S.-H. Park, Structural, morphological, optical, and magnetic properties of Gd-doped and (Gd, Mn) co-doped ZnO nanoparticles. Physica E, **93**, 111–115 (2017)
27. M. Nirmala, A. Anukaliani, Structural and optical properties of an undoped and Mn doped ZnO nanocrysatlline thin film. Photon. Lett. Poland **2**, 189–191 (2010)
28. B. Roy, S. Chakrabarty, O. Mondal, M. Pal, A. Dutta, Effect of neodymium doping on structure, electrical and optical properties of nanocrystalline ZnO. Mater. Charact. **70**, 1–7 (2012)
29. K.P. Misra, R. Shukla, A. Srivastava, A. Srivastava, Blueshift in optical band gap in nanocrystalline $Zn_{1-x}Ca_xO$ films deposited by sol-gel method. Appl. Phys. Lett. **95**, 031901 (2009)
30. M. Shkir, S. AlFaify, Tailoring the structural, morphological, optical and dielectric properties of lead iodide through Nd^{3+} doping. Sci. Rep. **7**, 16091 (2017)
31. S. AlFaify, M. Shkir, V. Ganesh, Facile one pot synthesis of novel Hg^{2+} doped PbI_2 nanostructures for optoelectronic and radiation shielding applications. Mater. Sci. Semicond. Process. **83**, 231–238 (2018)
32. K.D.A. Kumar, S. Valanarasu, V. Tamilnayagam, L. Amalraj, Structural, morphological and optical properties of SnS_2 thin films by nebulized spray pyrolysis technique. J. Mater. Sci. Mater. Electron. **28**, 14209–14216 (2017)
33. K.D.A. Kumar, S. Valanarasu, A. Kathalingam, K. Jeyadheepan, Nd^{3+} doping effect on the optical and electrical properties of SnO_2 thin films prepared by nebulizer spray pyrolysis for optoelectronic application. Mater. Res. Bull. **101**, 264–271 (2018)
34. A. Samy, E. Gomaa, N. Mostafa, Study the properties of Cu-Zn ferrite substituted with rare earth ions by using positron annihilation analysis. Open Ceram. Sci. J. **1**, 1–4 (2010)
35. S. Sharma, R. Kundu, A. Singh, S. Murugavel, R. Punia, N. Kishore, Structural, optical, electrical, and magnetic properties of $Zn_{0.7}Mn_xNi_{0.3-x}O$ nanoparticles synthesized by sol–gel technique. Cogent Phys. **2**, 1055623 (2015)
36. N. Vigneshwaran, S. Kumar, A. Kathe, P. Varadarajan, V. Prasad, Functional finishing of cotton fabrics using zinc oxide–soluble starch nanocomposites. Nanotechnology **17**, 5087 (2006)
37. A. Kaschner, U. Haboeck, M. Strassburg, M. Strassburg, G. Kaczmarczyk, A. Hoffmann, C. Thomsen, A. Zeuner, H. Alves, D. Hofmann, Nitrogen-related local vibrational modes in ZnO:N. Appl. Phys. Lett. **80**, 1909–1911 (2002)
38. G. Adamopoulos, A. Bashir, W.P. Gillin, S. Georgakopoulos, M. Shkunov, M.A. Baklar, N. Stingelin, D.D. Bradley, T.D. Anthopoulos, Structural and electrical characterization of ZnO films grown by spray pyrolysis and their application in thin-film transistors. Adv. Func. Mater. **21**, 525–531 (2011)
39. J. Tauc, R. Grigorovici, A. Vancu, Optical properties and electronic structure of amorphous germanium. Phys. Status Solidi (B) **15**, 627–637 (1966)
40. M. Shkir, I.S. Yahia, S. AlFaify, M.M. Abutalib, S. Muhammad, Facile synthesis of lead iodide nanostructures by microwave irradiation technique and their structural, morphological, photoluminescence and dielectric studies. J. Mol. Struct. **1110**, 83–90 (2016)
41. M. Shkir, Effect of titan yellow dye on morphological, structural, optical, and dielectric properties of zinc(tris) thiourea sulphate single crystals. J. Mater. Res. **31**, 1046–1055 (2016)
42. D. Zhao, S. Xu, M. Xie, S. Tong, H. Yang, Stress and its effect on optical properties of GaN epilayers grown on Si (111), 6H-SiC (0001), and c-plane sapphire. Appl. Phys. Lett. **83**, 677–679 (2003)
43. S. Rejitha, C. Krishnan, Synthesis of cadmium-doped copper oxide nanoparticles: optical and structural characterizations. Adv. Appl. Sci. Res. **4**, 103 (2013)
44. M. Anpo, M. Kondo, C. Louis, M. Che, S. Coluccia, Application of dynamic photoluminescence spectroscopy to the study of the active surface sites on supported molybdenum/silica catalysts: features of anchored and impregnated catalysts. J. Am. Chem. Soc. **111**, 8791–8799 (1989)
45. A. Ahmed, N.S. Gajbhiye, A.G. Joshi, Low cost, surfactant-less, one pot synthesis of Cu_2O nano-octahedra at room temperature. J. Solid State Chem. **184**, 2209–2214 (2011)
46. V. Roy, A. Djurišić, H. Liu, X. Zhang, Y. Leung, M. Xie, J. Gao, H. Lui, C. Surya, Magnetic properties of Mn doped ZnO tetrapod structures. Appl. Phys. Lett. **84**, 756–758 (2004)
47. D.J. Edison, W. Nirmala, K.D.A. Kumar, S. Valanarasu, V. Ganesh, M. Shkir, S. AlFaify, Structural, optical and nonlinear optical studies of AZO thin film prepared by SILAR method for electro-optic applications. Physica B **523**, 31–38 (2017)
48. V. Anand, A. Sakthivelu, K.D.A. Kumar, S. Valanarasu, A. Kathalingam, V. Ganesh, M. Shkir, S. AlFaify, I. Yahia, Rare earth Sm^{3+} co-doped AZO thin films for opto-electronic application prepared by spray pyrolysis. Ceram. Int. **44**, 6730–6738 (2018)
49. T.K. Gupta, Microstructural engineering through donor and acceptor doping in the grain and grain boundary of a polycrystalline semiconducting ceramic. J. Mater. Res. **7**, 3280–3295 (1992)
50. H.-J. Koo, M.-H. Whangbo, Magnetic superstructures of cupric oxide CuO as ordered arrangements of one-dimensional antiferromagnetic chains. Inorg. Chem. **42**, 1187–1192 (2003)
51. S. Rehman, A. Mumtaz, S. Hasanain, Size effects on the magnetic and optical properties of CuO nanoparticles. J. Nanoparticle Res. **13**, 2497–2507 (2011)

52. R. Gupta, K. Ghosh, L. Dong, P. Kahol, Green synthesis of hematite (α-Fe_2O_3) submicron particles. Mater. Lett. **64**, 2132–2134 (2010)
53. G.N. Rao, Y. Yao, J. Chen, Influence of Mn substitution on microstructure and magnetic properties of $Cu_{1-x}Mn_xO$ nanoparticles. J. Appl. Phys. **101**, 09H119 (2007)
54. F. Zhao, H. Qiu, L. Pan, H. Zhu, Y. Zhang, Z. Guo, J. Yin, X. Zhao, J.Q. Xiao, Ferromagnetism analysis of Mn-doped CuO thin films. J. Phys. Condens. Matter. **20**, 425208 (2008)
55. J. Coey, M. Venkatesan, C. Fitzgerald, Donor impurity band exchange in dilute ferromagnetic oxides. Nat. Mater. **4**, 173 (2005)
56. S. Kumar, P. Sahare, Nd-doped ZnO as a multifunctional nanomaterial. J. Rare Earths **30**, 761–768 (2012)
57. R. Bhowmik, N. Naresh, B. Ghosh, S. Banerjee, Study of low temperature ferromagnetism, surface paramagnetism and exchange bias effect in α-$Fe_{1.4}Ga_{0.6}O_3$ oxide. Curr. Appl. Phys. **14**, 970–979 (2014)